CrossMark

The multidecadal variations of the interannual relationship between the East Asian summer monsoon and ENSO in a coupled model

Bo Liu[1,4] · Gang Huang[1,3,4,5] · Kaiming Hu[1,2] · Renguang Wu[2] · Hainan Gong[2] · Pengfei Wang[1,2] · Guijie Zhao[1,2,6]

Abstract This study investigates the multidecadal variations of the interannual relationship between the East Asian summer monsoon (EASM) and El Niño-Southern Oscillation (ENSO) in 1000-year simulation of a coupled climate model. The interannual relationship between ENSO and EASM has experienced pronounced changes throughout the 1000-year simulation. During the periods with significant ENSO-EASM relationship, the ENSO-related circulation anomalies show a Pacific-Japan (PJ)-like pattern with significant wave-activity flux propagating from the tropics to the north in lower troposphere and from the mid-latitudes to the south in upper troposphere. The resultant ENSO-related precipitation anomalies are more (less) than normal over the East Asia (western North Pacific) in the decaying summers of El Niño events. In contrast, the circulation and precipitation anomalies are weak over East Asia-western North Pacific during the periods with weak ENSO-EASM relationship. Based on the energy conversion analysis, the related anomalies achieve barotropic and baroclinic energy from the mean flow during the periods with strong ENSO-EASM relationship. On the contrary, during the low-correlation periods, the energy conversion is too weak to form the link between the tropics and mid-latitudes. The main reason for the multidecadal variations of ENSO-EASM relationship is the amplitude discrepancy of SST anomalies over the Indo-western Pacific Ocean which, in turn, leads to the intensity difference of the western North Pacific anomalous anticyclone (WPAC) and related climate anomalies.

Keywords East Asian Summer monsoon · ENSO · Coupled climate model · Interannual · Multidecadal variations

✉ Gang Huang
hg@mail.iap.ac.cn

1 State Key Laboratory of Numerical Modeling for Atmospheric Sciences and Geophysical Fluid Dynamics, Institute of Atmospheric Physics, Chinese Academy of Science, 9804, Beijing 100029, China

2 Center for Monsoon System Research, Institute of Atmospheric Physics, Chinese Academy of Science, Beijing 100190, China

3 Joint Center for Global Change Studies, Beijing 100875, China

4 College of Earth Science, University of Chinese Academy of Sciences, Beijing 100049, China

5 Laboratory for Regional Oceanography and Numerical Modeling, Qingdao National Laboratory for Marine Science and Technology, Qingdao 266237, China

6 Beijing Meteorological Observatory, Beijing 100089, China

1 Introduction

The East Asian summer monsoon (EASM) is one of most dominant climate systems in East Asia, where includes most parts of China, Japan and Korea. The variability of EASM has great social and economic influences. Thus, understanding the processes for interannual to interdecadal variability of EASM is very crucial.

For the sake of perceiving and predicting the EASM variability, the monsoon index is a practical tool. There are more than 20 EASM indices and Wang et al. (2008b) stated that these indices can be divided into five groups. According to the difference of purposes, different indices can be used. The EASM index that we used in this paper is the one defined by Zhao et al. (2015) based on 200-hPa zonal wind. The EASM index chosen in this study is based on comprehensive consideration. There are many different indices to descript the East Asian summer monsoon variability, focusing on

different features, including rainfall, pressure, atmospheric circulation and the Meiyu front and so on. Previous studies have shown that the key processes of El Niño-Southern Oscillation (ENSO)'s impact on East Asia include a lower level anticyclone/cyclone in the Northwest Pacific (Wang et al. 2003; Xie et al. 2009) and upper circulation anomalies (Huang and Yan 1999). The index from Zhao et al. (2015) is selected because it properly contains not only the low-level and upper-level circulation anomalies in the Northwest Pacific, but also the related features over the mid-latitudes and tropics. This index can capture well the interannual and interdecadal variability of EASM. Moreover, it shows highly predictable in ENSEMBLES models. Hence, it is proper index to study the relationship between EASM and ENSO.

As many researches have indicated, one of the most important factors affecting EASM is ENSO (Chen et al. 1992; Zhang et al. 1999; Wang et al. 2000), the dominating mode in the tropical Pacific. The influence of ENSO events on EASM is indirect. In the decaying summer (June to August; JJA(1)) of El Niño events, an anomalous anticyclone appears over the western North Pacific (WPAC) (Zhang et al. 1996, 1999; Wang et al. 2003). Although this anomalous anticyclone restrains the convection over the western North Pacific, it brings abundant moisture on its west flank to East Asia from the tropics (Wang et al. 2000; Wu and Kirtman 2003). Zhang et al. (1996) considered an atmospheric Rossby wave response induced by the western tropical Pacific convective cooling anomalies as the main reason of the generation of WPAC during the El Niño mature phase. Wang et al. (2000) proposed a wind-evaporation-SST (WES) feedback mechanism to explain the development and maintenance of WPAC from the El Niño matured winter to the following summer. Some other researches tend to consider the tropical Indian Ocean warming as the dominant contributor of the WPAC (Yang et al. 2007; Wu et al. 2009; Xie et al. 2009). Moreover, the Indo-western Pacific Ocean capacitor (IPOC) effect is presented by Xie et al. (2016), who systematically explained and synthesized the theories that emphasized roles of SST cooling over the western North Pacific and SST warming over the North Indian Ocean. The IPOC effect reveals that both mechanisms are available just in a two-stage evolution. Recently, Zhang et al. (2017) summarized major achievements about the impact of El Niño on the interannual variability of atmospheric circulations over East Asia through the WPAC, and how the WPAC is maintained from winter when El Niño is in its peak to the following summer by multiple factors.

As ENSO is an important factor in seasonal prediction of summer precipitation over the East Asia, understanding the relationship between ENSO and EASM has its great values. However, the relationship is not stationary and shows significant decadal variations according to analysis of limited observational data and the phase 5 of the Coupled Model Intercomparison Project (CMIP5) outputs (Wu and Wang 2002; Wang et al. 2008a; Huang et al. 2010; Xie et al. 2010; Hu et al. 2014). The relationship of EASM and ENSO experienced an interdecadal change around the late 1970s (Wu and Wang 2002; Wang et al. 2008a; Xie et al. 2010; Huang et al. 2010). Wu and Wang (2002) mentioned that the increase of summer mean SST in the Philippine Sea after the 1970s may change the location and intensity of anomalous convection over the western North Pacific, which induces the decadal variation of the relationship between EASM and ENSO. Using observational data and atmospheric general circulation model (AGCM), Xie et al. (2010) emphasized the role of SST change in the tropical Indian Ocean in the atmospheric response to ENSO. The change in the magnitude and period of ENSO and monsoon-ocean interaction variation may also have contribution to the decadal variations (Wang et al. 2008a). In addition, Song and Zhou (2015) showed that the internal variability is the most important factor in the decadal change. However, previous researches about the decadal variations have their own drawbacks and are restricted by the limited available time of the observational data. In this paper, a 1000 year control run in a coupled climate model is used to study the multidecadal variations of the relationship between ENSO and EASM and its possible mechanisms.

The rest of this paper is organized as follows. The model and data used in this paper are introduced in Sect. 2. The results of multidecadal variations of the interannual relationship between EASM and ENSO and its circulation anomalies are described in Sect. 3. The possible mechanism for the multidecadal variations is analyzed in Sect. 4. Section 5 summarizes the main results.

2 Model, data and analysis methods

In this study, we used output from a coupled model, called the integrated coupled model (ICM). The ICM is an atmosphere-ocean-sea ice coupled general model without flux adjustment, which is developed at the Center for Monsoon System Research, Institute of Atmospheric Physics (CMSR/IAP), Chinese Academy of Sciences, since 2008. This model integrates the Hamburg Atmospheric General Circulation Model Version 5 (ECHAM5) (Roeckner and Coauthos 2003) and the Nucleus for European Modeling of the Ocean Version 2.3 (NEMO 2.3) (Madec 2008) using the Ocean Atmosphere Sea Ice Soil Version 3 (OASIS3) (Valcke 2006) as the coupler. Its framework is similar to the Kiel Climate Model (KCM) (Park et al. 2009) and SINTX (Gualdi et al. 2003; Luo et al. 2005). ICM can well reproduce the distribution of precipitation and sea surface temperature (SST), and the ENSO-related summer climate over East Asian-western North Pacific is successfully simulated too (Huang et al. 2014). More details of ICM can be

found in Huang et al. (2014). Moreover, a new version of ICM (ICM.V2) has been developed through many researches' joint efforts (Liu et al. 2017). The new version has improvements in simulating mean state of SST and precipitation, and has more realistic ENSO cycle and effects on the East Asian summer climate. The ICM.V2 simulated seasonal cycle of SST deviation from the annual mean over the equatorial Pacific is quite similar to that in observations. The correlation coefficient of the seasonal evolution of SST deviation along the equatorial Pacific reaches 0.67 between the ICM.V2 and the observations. The power spectrum of Niño3 SST anomalies displays a peak around 3.75-year in the observations and 3.33-year in the ICM.V2. The standard deviation of decadal variation of the EASM index obtained by 21-year running mean is about 1.7 in the model, compared to 1.2 in the observations. The ENSO-related SST anomalies in the equatorial Pacific decay slower in the ICM.V2 than in the observations (Huang et al. 2014; Liu et al. 2017), which is a common bias in most of the coupled general circulation models (GCMs). In this paper, the ICM.V2 is used as it has a good performance in simulating the characters of ENSO and EASM and is a proper model to study the EASM-ENSO relationship. The data we used here is the 1000 years control experiment.

In order to verify the conclusion we made, an AGCM named ECHAM5, the Hamburg version of the European Centre for Medium-Range Weather Forecasts (ECMWF) model (Roeckner et al. 2006), is used for our subsequent several sensitive experiments. We employ the version of ECHAM5 with triangular truncation at zonal wave number 63 (T63) and 19 sigma levels in the vertical.

A Niño-3.4 index, which is used to represent ENSO events in this paper, is computed by averaging the December-February (DJF) SSTs over the domain of 5°S–5°N, 120°–170°W. The EASM index (Zhao et al. 2015) is calculated by

$$EASMI = Nor(u(2.5° - 10°N, 105° - 140°E)$$
$$- u(17.5° - 22.5°N, 105° - 140°E)$$
$$+ u(30° - 37.5°N, 105° - 140°E)).$$

Here, *Nor* represents normalized and u is the JJA mean of 200-hPa zonal wind.

To make clear of the energy conversion from mean state to anomalous fields, barotropic and baroclinic energy conversions analyses are applied. The local barotropic energy conversion CK associated with the normalized previous DJF Niño-3.4 index is calculated following the formula provided by Hoskins et al. (1983) and Simmons et al. (1983):

$$CK = \frac{v'^2 - u'^2}{2}\left(\frac{\partial \bar{u}}{\partial x} - \frac{\partial \bar{v}}{\partial y}\right) - u'v'\left(\frac{\partial \bar{u}}{\partial y} + \frac{\partial \bar{v}}{\partial x}\right).$$

Here, u' and v' represent the ENSO-related zonal and meridional wind anomaly, respectively, $\bar{u}$ and $\bar{v}$ respectively represent the mean state of zonal and meridional wind.

Positive CK implies the conversion of kinetic energy from the mean flow to the anomalies associated with the ENSO.

The vertical integral of local baroclinic energy conversion (CP) is based on the following equation (Kosaka and Nakamura 2006):

$$CP = -\left[\frac{f}{\sigma}v'T'\frac{\partial \bar{u}}{\partial p} - \frac{f}{\sigma}u'T'\frac{\partial \bar{v}}{\partial p}\right].$$

Here, T', u' and v' is the temperature, zonal and meridional wind anomaly in each altitude associated with the normalized previous DJF Niño-3.4 index, respectively. $\bar{u}$ and $\bar{v}$ are the same as which in the equation CK but contains vertical dimension, σ denotes $\sigma = \frac{R\bar{T}}{c_p p} - \frac{d\bar{T}}{dp}$. In addition, the square bracket represents a vertical integral from the surface to 100-hPa level.

Throughout this paper, analysis methods include regression, correlation and physical analysis. The significant levels are computed with the standard two-tailed Student's t test.

3 The multidecadal variations of EASM-ENSO relationship

In order to investigate decadal variation in the interannual relationship between EASM and ENSO, 21-year sliding correlation method is applied. Figure 1 shows the 21-year sliding correlation between previous boreal winter (DJF) Niño-3.4 index and EASMI in a 1000-year control run. The correlation shows obvious multidecadal variations, ranging from −0.22 to 0.78, indicating an unstable relationship between EASM and ENSO. This phenomenon is similar to that obtained based on observations and CMIP5 data (Hu et al. 2014; Song and Zhou 2015), but the range of the correlation coefficient in ICM is relatively bigger than that in the observations. As indicated by Hu et al. (2014), not all CMIP5 models can capture this unstable relationship. Therefore, ICM, the model used in present study, is quite suitable for analyzing the multidecadal variations in the EASM-ENSO relationship.

According to the 21-year sliding correlation, we choose two sets of periods from the 1000 year run for composite analysis. One is the high correlation periods (red curve segments in Fig. 1), and another is the low one (blue curve segments in Fig. 1). Both include 10 21-year periods, constituting 210 years. It is worth to mention that the low correlation periods are chosen from the 21-year sliding correlation coefficient close to zero to obtain the greater difference between the high- and low-correlation periods in corresponding circulation patterns. The following analysis is all based on these two sets of data except for additional notice.

Fig. 1 The 21-year sliding correlation between Niño-3.4 index in the previous winter and the EASM index during 1-1000 years in ICM model. The dashed line indicates running correlation significant at the 5% level. The red (blue) curve segments represent the high (low)-correlation periods we choose with green (yellow) solid circles in their middle years
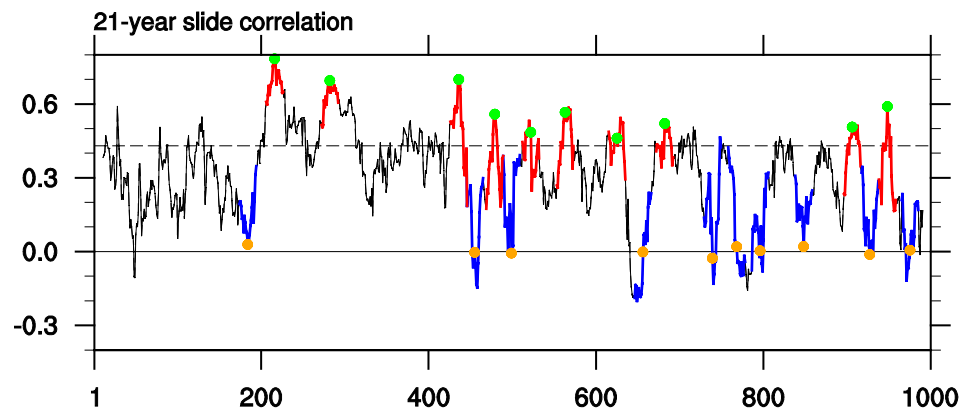
3.1 Precipitation anomaly

Based on the selected two types of periods, the corresponding spatial patterns of JJA(1) precipitation regressed onto normalized previous DJF Niño-3.4 index over the Indo-Pacific are shown in Fig. 2. During the high-correlation periods (Fig. 2a), the distribution of JJA(1) precipitation shows a distinct tripole meridional pattern over the tropical and mid-latitude of the western Pacific, with two obvious positive rain anomaly bands located over the western tropical Pacific and Meiyu-Changma-Baiu region which extends from the Yangtze River valley in China to east of Japan, and negative rainfall anomaly located in between. By contrast, the magnitude of precipitation anomalies over
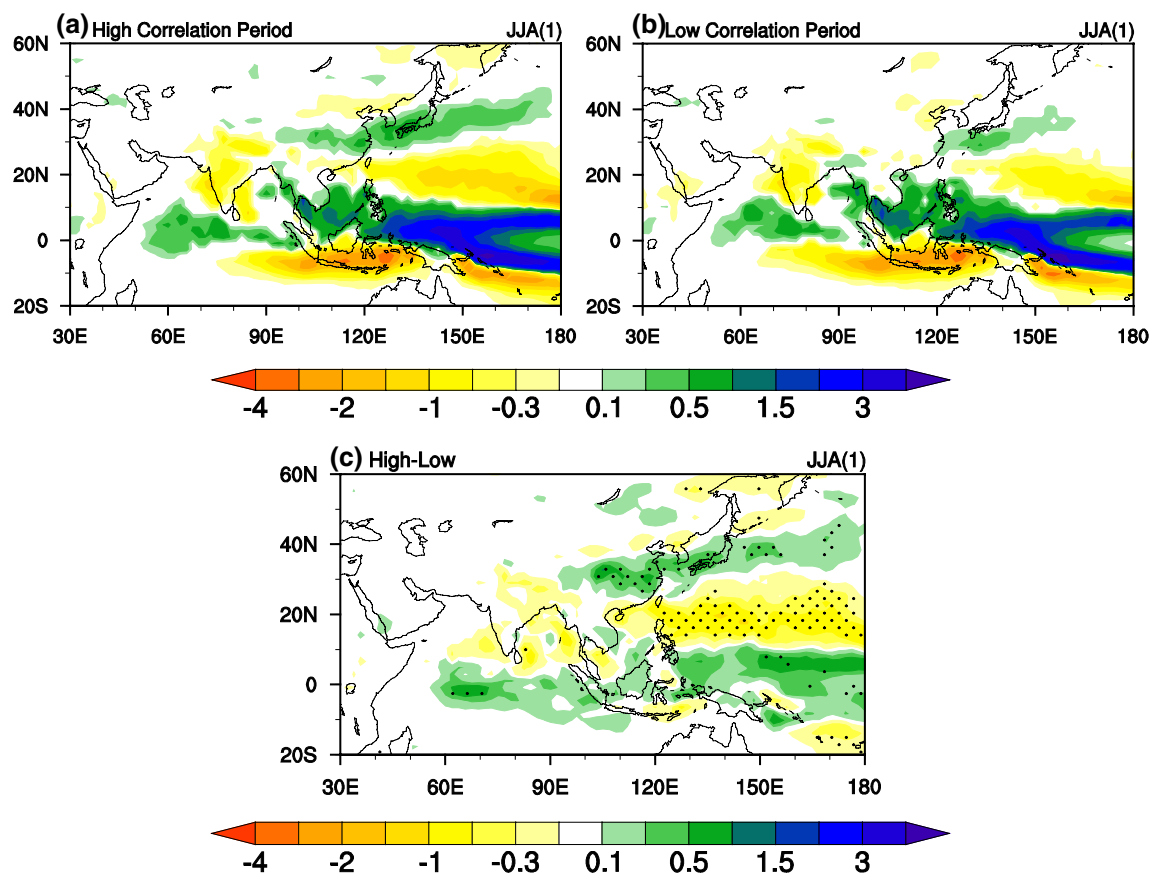
Fig. 2 The regression pattern of JJA(1) precipitation with respect to normalized previous winter Niño-3.4 index for **a** high- and **b** low-correlation periods and **c** its difference. The **a, b** shaded and **c** dotted on the map indicate precipitation are significant at the 5% level using Student's *t* test

the tripole rain bands is smaller during the low-correlation periods (Fig. 2b), especially in the mid-latitudes. As such, the difference of the precipitation anomalies between the high-correlation and low-correlation periods display a distribution of more precipitation in Meiyu-Changma-Baiu rain bands and less precipitation over the western subtropical North Pacific around 10°–30°N (Fig. 2c).

3.2 Circulation anomaly

The spatial patterns of JJA(1) 850-hPa wind and SLP associated with the normalized previous DJF Niño-3.4 index are shown in Fig. 4. During the high-correlation periods, an evident anomalous anticyclone extends from the western North Pacific to east of China in the low-level, with a relative weak cyclone anomaly located to its north (Fig. 3a). The northwest flank of the anomalous anticyclone is a region of convergence between anomalous southerly and northerly winds, which induces more precipitation there (Fig. 2a). The anomalous wind distribution is characterized by a Pacific-Japan (PJ; Nitta 1987)-like pattern with a positive SLP anomaly over the western North Pacific around 20°–30°N

and a negative anomaly in its north around 30°–40°N. This dipole SLP anomaly pattern is similar to the results of Song and Zhou (2015) who selected 4 sets of periods based on the 20CR observational data (Compo et al. 2011). However, the dipole SLP anomaly pattern disappears and the low-level anomalous anticyclone is weak during the low-correlation periods (Fig. 3b). From the distribution of difference between the two periods (Fig. 3c), we can clearly find that the main circulation discrepancy between these two periods lies over the western North Pacific and is similar to the pattern in the high-correlation periods.

From analyzing JJA(1) 200-hPa wind and 500-hPa omega anomalies associated with the normalized previous DJF Niño-3.4 index for high- and low-correlation periods (Fig. 4), we can find that the differences between the two periods in the high-level of troposphere are mainly concentrated on the following aspects. First, the upper-level wind anomalies show zonally elongated pattern in the high latitudes over northeast China and the North Pacific, and feature a meridional wave structure in the high-correlation periods (Fig. 4a). In the low-correlation periods, there is no clear signal over the high latitude (Fig. 4b). Second, the 200-hPa
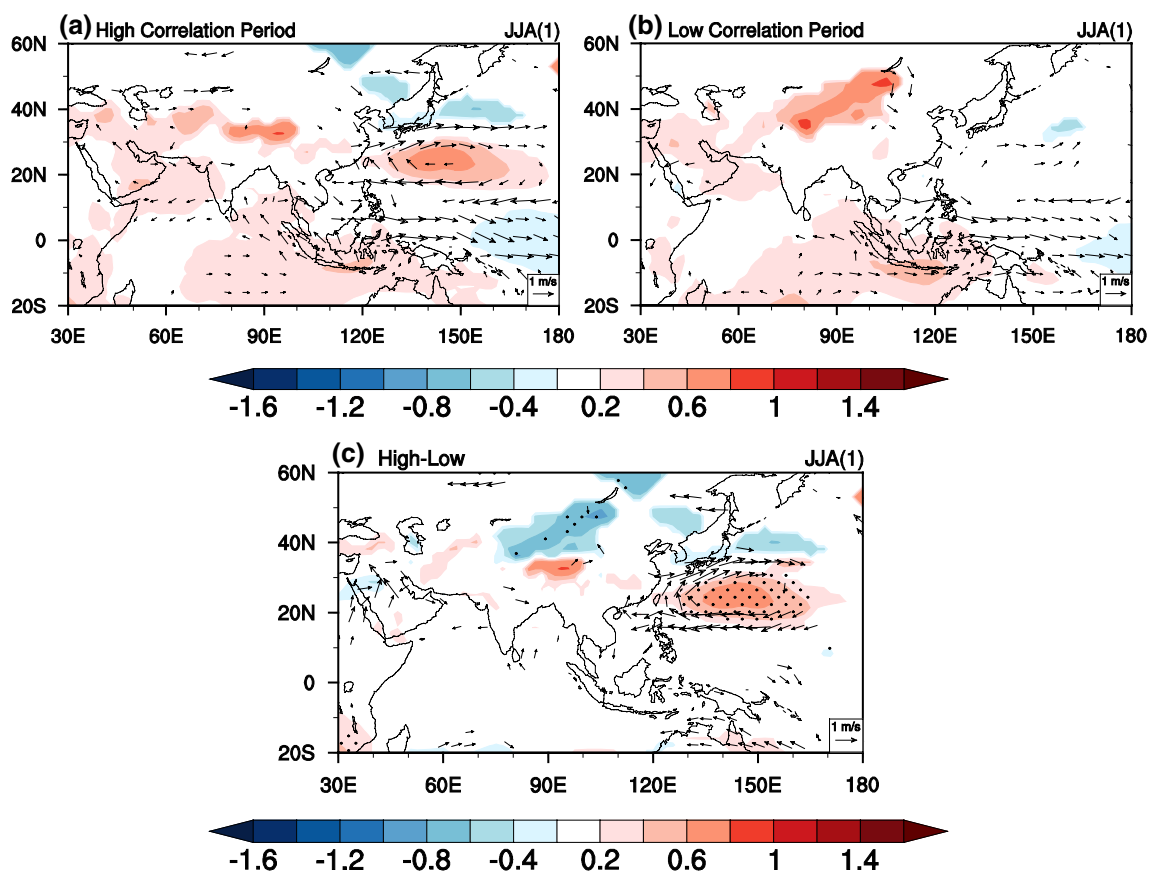
Fig. 3 The JJA(1) SLP (shaded; hPa) and 850-hPa wind (vector; m s^{-1}) regressed onto previous winter Niño-3.4 index for **a** high- and **b** low-correlation periods and its difference (**c**). The **a, b** shaded and **c** dotted on the map indicate SLP is significant at the 5% level using Student's *t* test. The 850-hPa wind is shown when meridional or zonal component is significant at the 5% level using Student's *t* test
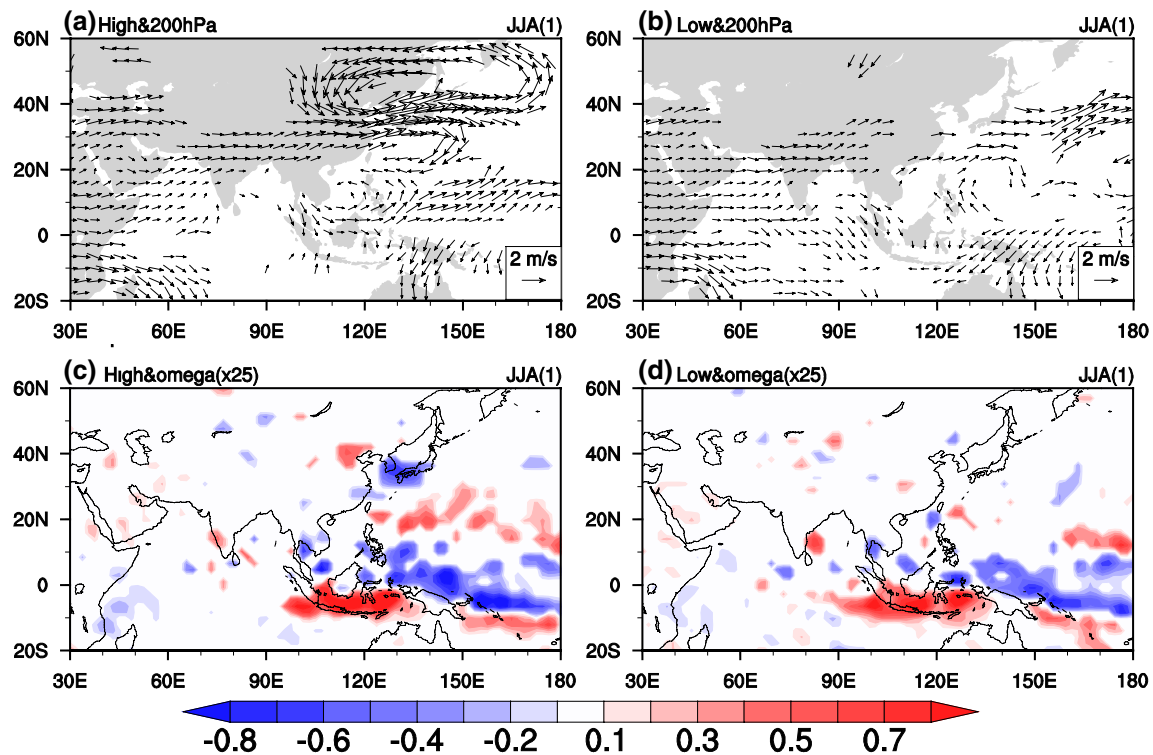
Fig. 4 The **a, b** 200-hPa wind (m s^{-1}), and **c, d** 500-hPa omega ($\times$25; Pa s^{-1}), regressed onto normalized previous winter Niño-3.4 index for **a, c** high- and **b, d** low-correlation periods. The wind is shown when the meridional or zonal component is significant at the 5% level using Student's *t* test

circulation pattern is similar to that at the low-level (Fig. 3a), indicating a quasi-barotropic structure in the mid-latitudes but with stronger anomalous anticyclone over the western North Pacific extending westwards to inland China that has greater influences on the East Asian climate. During the low-correlation periods, the anticyclone anomaly over the western North Pacific is much weaker and located more eastward (Fig. 3b). Third, there are significant negative omega anomalies (ascending motions) over east China, Korea and south Japan in the high-correlation periods (Fig. 4c), whereas the vertical motion anomaly is weak or absent in the low-correlation periods (Fig. 4d). Therefore, abundant moisture is brought by the southwesterly anomaly over the west flank of the low-level anomalous anticyclone and modulated by the high-level circulation, leading to more precipitation over the western North Pacific, especially over the Meiyu-Changma-Baiu rain bands in the high-correlation periods.

3.3 Vorticity anomaly and wave activity flux

To investigate the propagation of the stationary Rossby waves, the horizontal components of wave-activity flux defined by Takaya and Nakamura (2001) is evaluated in our study. The regression of JJA(1) (a) 200-hPa and (b) 850-hPa vorticity onto the normalized previous DJF Niño-3.4 index

and corresponding wave-activity flux during the two periods are shown in Fig. 5.

During the high-correlation periods, in the lower troposphere (Fig. 5a), the main positive vorticity anomalies are located over the Tropics and mid-latitudes around 30°–40°N. From the vorticity budget point of view, the positive vorticity anomaly is a local response to anomalous heating. Positive vorticity indicates the enhanced convection. The dominant negative vorticity anomaly is concentrated over the western North Pacific around 20°–30°N. These vorticity anomalies display a meridional structure from the Tropics to mid-latitudes. In the high-level troposphere (Fig. 5b), the primary positive vorticity anomalies are located over the north-east of China and north of Japan. Moreover, a relative small positive vorticity exists over the west tropical Pacific around 150°E. Between these two positive anomalies, there has a zonal elongated negative vorticity anomaly over the western North Pacific. Compared to the low-level troposphere, the corresponding vorticity anomalies display a northward displacement. During the low-correlation periods, the vorticity anomalies are much smaller at both low-level and upper-level (Fig. 5c, d).

In addition, the stationary Rossby wave activity flux is shown in Fig. 5. During the high-correlation periods, in
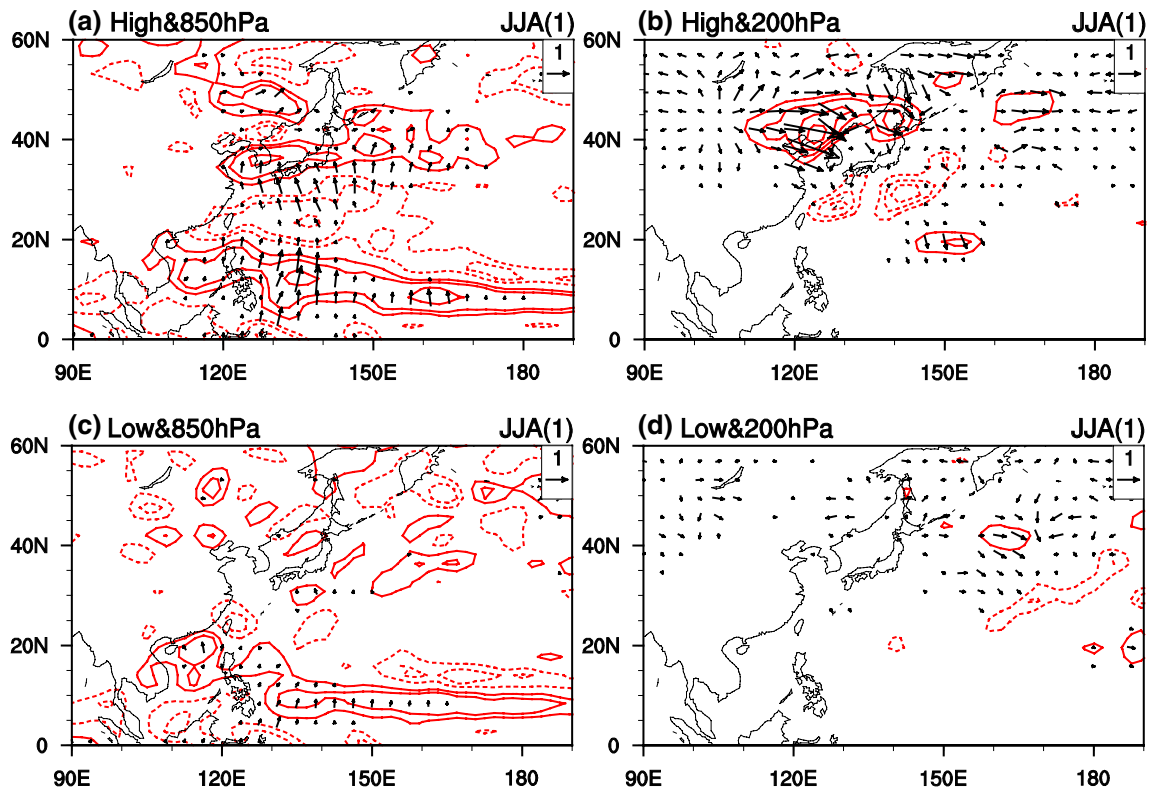
Fig. 5 The regression of **a, c** 850-hPa and **b, d** 200-hPa vorticity (contour; units: $\times 10^{-6}$ s^{-1}) in JJA onto DJF Niño3.4 index and corresponding wave activity flux (vector; units: m^2 s^{-2}) during the **a, b** high-correlation and **c, d** low-correlation periods. The contours are $\pm 4, \pm 6, \pm 8, \pm 10$ in **a, c** and $\pm 1, \pm 2, \pm 4, \pm 6$ in **b, d**; respectively

the low-level troposphere (Fig. 5a), the wave activity fluxes point from the Tropics northward to high-latitude area, which corresponds well with the anomalous vorticity. In contrast, in the 200-hPa (Fig. 5b), the wave activity fluxes tend to be in opposite direction, from the North to South. During the low-correlation periods, the wave activity flux has no significant signal except for lower-level tropics of the western Pacific (Fig. 5c, d).

As a whole, during the high-correlation periods, the low-level and upper-level wave activity fluxes appear to suggest a positive feedback between the tropics and mid-latitudes. A perturbation over the western tropical Pacific in lower troposphere would trigger a wave train extending to the mid-latitudes, and in turn the mid-latitude signal propagates to the south in the upper troposphere, and these processes form a significant positive feedback that intensifies the western North Pacific anticyclone anomaly.

4 The possible causes for the multidecadal variations on EASM-ENSO relationship

To investigate how SST anomaly affects the atmospheric circulation, the seasonal evolution of SST anomalies is

shown in Fig. 6. In the previous D(0)JF(1), the anomalous SST is characterized by El Niño-like pattern, with positive SST anomaly over the central and eastern Pacific, and two regions of negative anomalies off the western equatorial Pacific (Fig. 6a). Through subtracting the SST anomalies in the two periods, we can find significant differences over the eastern Tropical Pacific (Fig. 6d). Compared to the low-correlation periods, the high-correlation periods have warmer SST anomaly in the region south of equator, indicating that the strength of ENSO has been relatively reinforced, and the Walker circulation could be weakened over the Tropical area. The SST difference pattern moves westward and displays a cooling over the tropical western Pacific in MAM(1) (Fig. 6e). This indicates that the SST cooling off the tropical western Pacific is decaying more slowly during the high-correlation periods than during the low-correlation periods. In JJA(1), the positive SST anomaly difference in the western equatorial Pacific indicates that the model warm events are decaying slower than observations. This is a common bias present in most of coupled GCMs (Kim and Yu 2012; Bellenger et al. 2013; Gong et al. 2015), which may weaken the response of the Northwest Pacific summer monsoon to ENSO (Jiang et al. 2017). Although positive SST anomaly has gradually decayed over the Tropical Pacific, the Indian
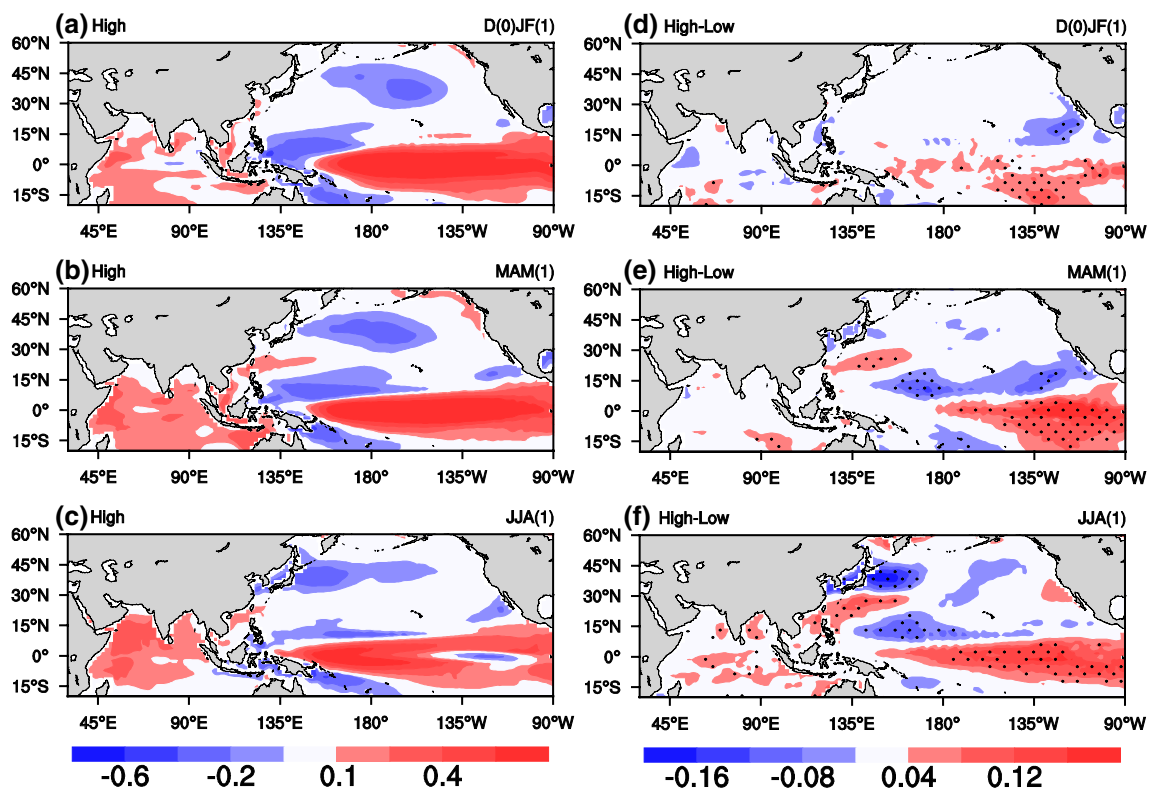
Fig. 6 The **a** D(0)JF(1), **b** MAM(1) and **c** JJA(1) SST (shaded; °C) regressed onto the normalized previous winter Niño-3.4 index for high-correlation periods and their differences between high- and low-

correlation periods in **d** D(0)JF(1), **e** MAM(1) and **f** JJA(1), respectively. The black dots indicate SST is significant at the 5% level using Student's *t* test

Ocean warming is still strong (Fig. 6c), which is due to weakening of surface wind and evaporation as anomalous winds are against the prevailing southwesterly winds over the North Indian Ocean according to the wind-evaporation-SST (WES) feedback mechanism (Xie and Philander 1994; Wu et al. 2008; Du et al. 2009). Relatively speaking, the SST in the central and northern Indian Ocean, and South China Sea is significant warmer during the high-correlation periods than that during the low-correlation periods (Fig. 6f). The difference of SST anomalies over the western Pacific could be related to the pace of ENSO decaying (Tao et al. 2015; Jiang et al. 2017). Different coupled GCMs from CMIP5 have the different pace of decay of ENSO events, which might relate to the unrealistic simulation of the cold tongue in models (Jiang et al. 2017). Based on previous studies, the Indian Ocean warming plays an important role in WPAC. However, the significant SST anomaly difference in the tropical Indian Ocean between the two periods is scattered. As such, the role of Indian Ocean warming might not the only reason caused the WPAC. Hence, we here hypothesis that the WPAC may be more strengthened by the combined functions of the Indian Ocean and the western tropical Pacific.

4.1 Indo-Western Pacific Ocean capacitor effect

To verify the above hypothesis and understand the possible reason of the multidecadal variations in interannual relationship between EASM-ENSO, first, we investigate the impact of the concurrent JJA(1) Indo-Western Pacific Ocean SST anomalies. The correlation of JJA(1) SST and 200-hPa geopotential height on normalized previous DJF Niño-3.4 are shown in Fig. 7. Based on the observations, the 200-hPa geopotential height anomalies display a Matsuno-Gill pattern (Matsuno 1996; Gill 1980) over the tropical Indian Ocean, with a Kelvin wave trough eastward to the equatorial western Pacific and two Rossby wave tails in the western Indian Ocean (Xie et al. 2009). There will be apparent response in the upper troposphere when the Indian Ocean warms up. The maximum positive correlation for SST during both two periods is located over the north Indian Ocean and the tropical western Pacific, but the correlation is higher during the high-correlation periods than during the low-correlation periods over the southwest tropical Indian Ocean, the north Indian Ocean and South China Sea. In contrast, the correlation over the tropical western Pacific is higher during the low-correlation periods. Another greater difference is located off the tropical western Pacific where the high-correlation
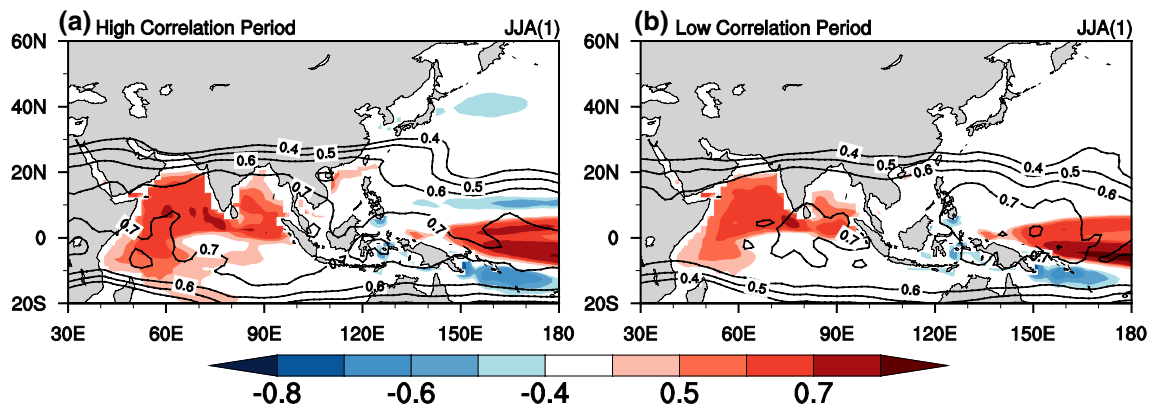
Fig. 7 The correlation of JJA SST (shaded) and 200-hPa geopotential height (contours for correlation equal or greater than 0.4) with DJF Niño-3.4 in **a** high- and **b** low-correlation periods

periods have colder SST anomaly than the low-correlation periods. Furthermore, the 200-hPa geopotential height correlation pattern displays a significant Matsuno-Gill pattern over the Indian Ocean during the high-correlation periods, with a Kelvin wave wedge penetrating to the western North Pacific (Fig. 7a). During the low-correlation periods, the wave extension to the western North Pacific is not obvious (Fig. 7b). Hence, the SST anomalies over the Indian Ocean and tropical western Pacific could play important roles in the strengthening of WPAC to modulate the multidecadal variations of EASM-ENSO relationship. Hu et al. (2014) have shown that the Indian Ocean warming has great impacts on the WPAC. Therefore, we will use an AGCM to further confirm the importance of SST anomalies over tropical western Pacific in the next subsection.

4.2 Sensitive experiment in an atmospheric general circulation model

In this subsection we use an AGCM to investigate the hypothesis that the multidecadal variations of the interannual relationship between EASM-ENSO is mainly caused by the tropical SST change not only in the Indian Ocean but also in the tropical western Pacific. The model we used here is ECHAM5.4, which has a good performance in simulating the East Asian Summer Climate (Song and Zhou 2014). Here, we have performed five experiences, named EXP_CON, EXP_HP, EXP_LP, EXP_CEP and EXP_P. In EXP_CON run, the specified SST forcing is climatological monthly mean SST. In EXP_HP run, the SST forcing is the SST anomalies over the Tropical Ocean area (20°S–20°N), which are double the regression of monthly SST anomalies from January to August on its normalized D(0)JF(1) Niño-3.4 index during the high-correlation periods, added on the observed monthly climatology SST which is the same as in EXP_CON. In EXP_LP run, SST forcing is similar

to EXP_HP but the SST anomalies are obtained from the low-correlation periods. The difference of the SST forcing between EXP_HP and EXP_LP is mainly located over the western tropical Pacific from January to May, with less difference over the Indian Ocean (Fig. 8a–e). When comes to JJA (Fig. 8f–h), the anomalous SST over the tropical Indian Ocean is relatively enhanced but still scattered. Therefore, the difference of these two sensitive experiments can explain the main effects of the SST discrepancy over the western tropical Pacific. In the last two experiments, the anomalous SST forcing is only imposed over the tropical Pacific Ocean. Specifically, the difference of SST anomalies between EXP_HP and EXP_LP (Fig. 8) over the whole tropical Pacific added on EXP_CON are used to force the EXP_P experiment. But in the EXP_CEP experiment, only the positive SST anomalies over the central and eastern tropical Pacific are added. The purpose of the last two experiments is to examine the contribution of SST anomalies in central and eastern equatorial Pacific. It is worthy to mention that the period of the added anomalous SST is only executed from January to August and run for 30 year in all experiments.

Figure 9 shows the spatial distribution of JJA mean precipitation and 850-hPa wind and the difference between these five experiments. In Fig. 9b, we can see an apparent meridional distribution of precipitation difference over the western Pacific, corresponding well with a meridional distribution of difference in 850-hPa wind. Over East Asia, especially Korea and Japan, more precipitation occurred in the EXP_HP, which is related to a cyclone anomaly, and an anticyclone anomaly appears over the western North Pacific. The above feature is well matched in the Northwest Pacific east of 140°E with the significant difference between previous high- and low-correlation periods (Fig. 2c). One exception is the South China Sea where there is a strong air-sea interaction (He and Wu 2013). The difference of rainfall anomalies in the
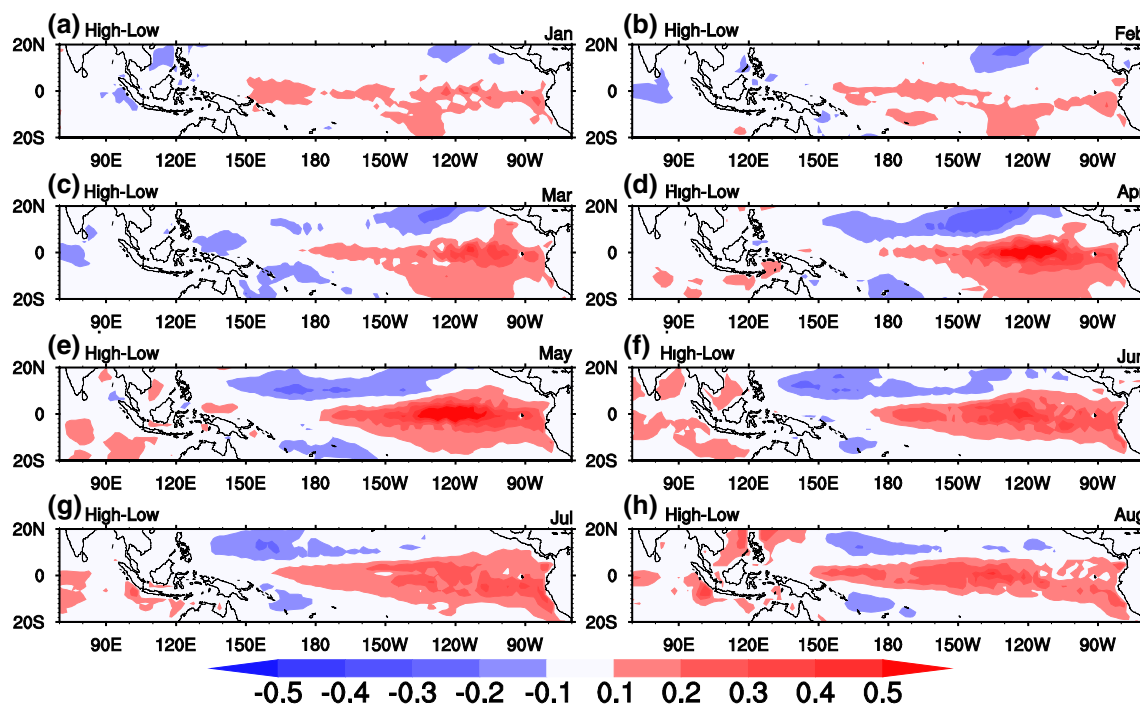
Fig. 8 Difference of monthly averaged SST (shaded; °C) forcing between EXP_HP and EXP_LP atmospheric GCM runs arranged from **a** January to **h** August in order. The SST forcing of EXP_P and EXP_CEP are partly of those in **a**–**h** but which over the whole Pacific and only the positive SST in Pacific, respectively
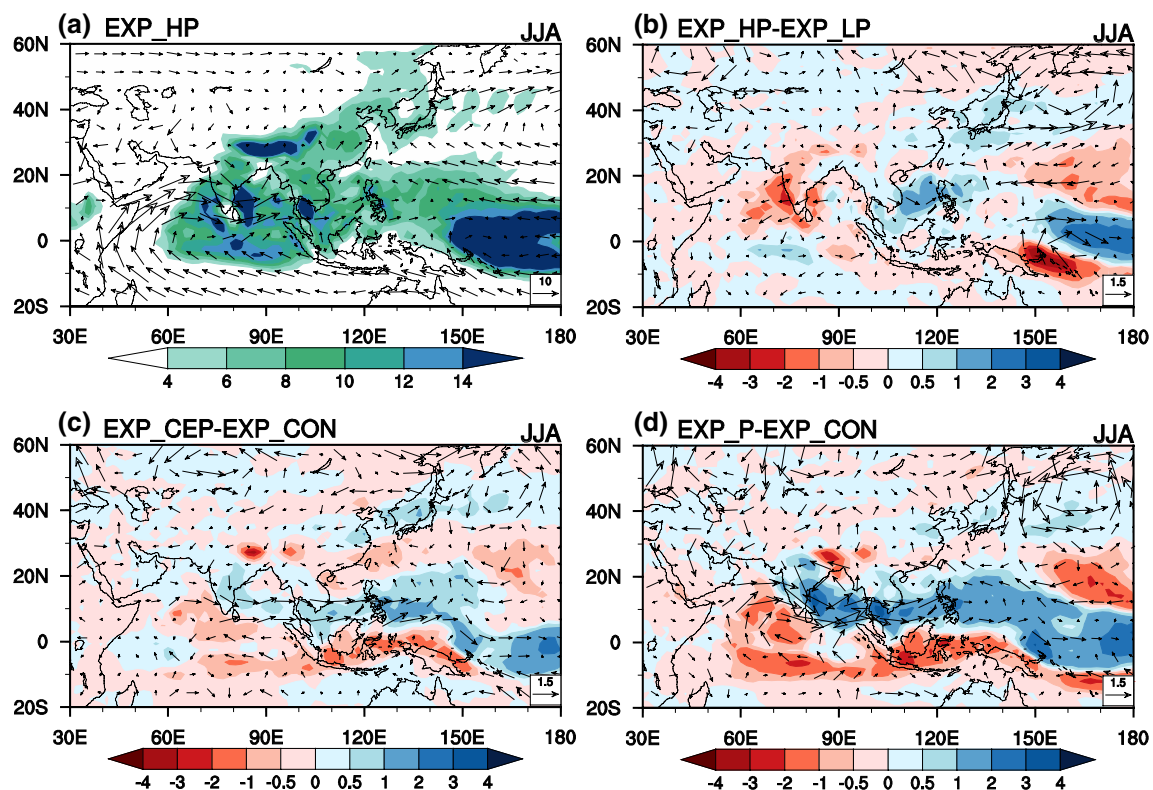
Fig. 9 The spatial pattern of precipitation (shaded; mm day^{-1}) and 850-hPa wind (vector; m s^{-1}) on climatological JJA mean state in the **a** EXP_HP and their difference (**b**) between the EXP_HP and EXP_LP, **c** EXP_CEP and EXP_CON, and **d** EXP_P and EXP_CON, respectively

South China Sea probably result from difference between coupled and SST forced simulations. As shown in Fig. 8, there are positive SST anomalies in the South China Sea, which may be forced by anticyclonic atmospheric circulation and negative rainfall anomalies there (Fig. 2c) according to He and Wu (2013). While in the AGCM, these positive SST anomalies may produce positive rainfall anomalies, different from the observations. Overall, we may hence draw a conclusion that the previous tropical SST anomalies, especially SST anomalies over the Indo-western tropical Pacific, play an important role in the circulation differences between different decades of inter-annual relationship between EASM and ENSO. Which region of anomalous SST is the uppermost contributor? From the differences between EXP_CEP (Fig. 9c), EXP_P (Fig. 9d) and EXP_CON, we can see that the contribution of SST anomalies in the central and eastern tropical Pacific where the 850-hPa wind field over East Asia shows a cyclone structure (Fig. 9c) is opposite to the main effect of the whole tropical Pacific (Fig. 9d), indicating its negative effect on WPAC. Moreover, the effect of anomalous SST over tropical Pacific (Fig. 9d) on the western Pacific circulation pattern is quite similar to that over the whole tropical Ocean (Fig. 9b), verifying the above hypothesis that the main contributor for the WPAC is the SST anomalies over the tropical Pacific, especially the cold SST anomalies off the tropics. In addition, comparing the results of five experiments, some other conclusions can also be found about Indian Ocean. First, the local effect of SST anomalies over tropical Indian Ocean forces a positive and negative rainfall pattern from the tropics to its north associated with warm SST anomalies in the equator. Through analyzing the 850-hPa wind field, the anomalous SST over the tropical Indian Ocean motivates northeasterlies anomalies, which favor the Indian Ocean warming by reducing the climatological westerly winds according to the WES feedback mechanism (Fig. 9b), which is apparently opposite to the only Pacific SST forcing experiments (Fig. 9c, d). Moreover, the Indian Ocean SST anomaly displays a teleconnection with the western Pacific summer climate from comparing Fig. 9b, d.

From the above sensitive experiments, we can make a conclusion that the SST anomalies of Indo-western Pacific play essential roles on the WPAC. This agrees with Wu et al. (2014) that demonstrated a combined effect of an east–west SST anomaly contrast between the North Indian Ocean and the central North Pacific on the WPAC in summer through AGCM experiments. Another question is how the anomalous systems develop and maintain. In the following, we consider and discuss them from the energy conversion standpoint.
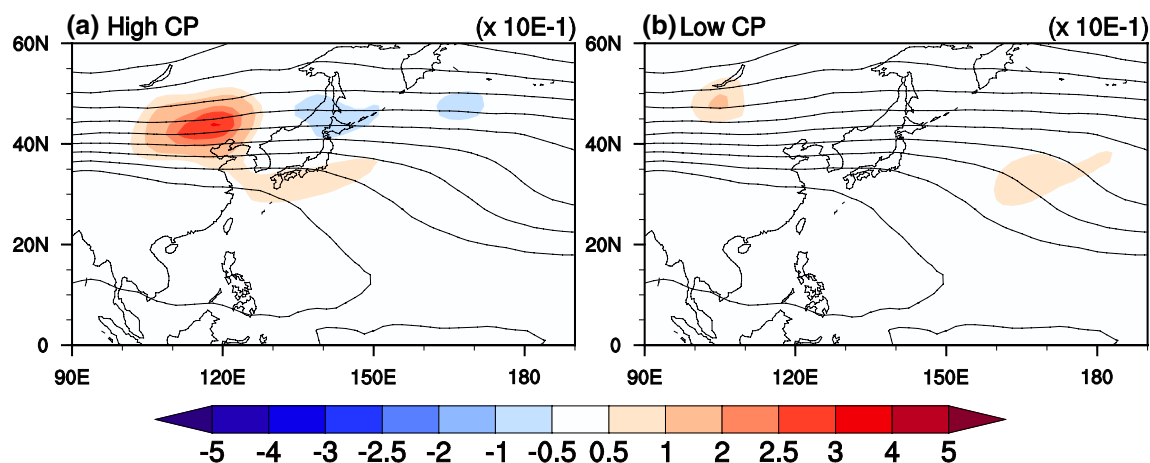
4.3 Energy conversion

In order to make clear the source of the energy to maintain the anomalous climate system, we further investigate the barotropic and baroclinic energy conversions during the high- and low-correlation periods. Figure 10 shows the spatial distribution of CK at the 850- and 200-hPa levels. The horizontal component of the extended Eliassen-Palm (EP) flux $\vec{E} = \left(v'^2 - u'^2, -u'v'\right)$ is also estimated and shown. During the high-correlation periods, positive CK is mainly concentrated in the tropics and negative CK in south of Japan and the South China Sea in the lower troposphere (Fig. 10a). The positive CK over the tropics is consistent with the result by Kosaka and Nakamura (2006). Over the western North Pacific, the negative CK is mainly contributed by the anomalous northeasterlies ($u'v' > 0$) in the entrance of the southwesterly jet ($\partial \bar{u}/\partial y > 0$). In the upper troposphere (Fig. 10b), the spatial pattern of CK has an apparent zonal distribution in mid-latitude area. Over northern China and east of Japan are positive CK, and between these regions there is a negative CK center. Owing to the location in the exit of subtropical jet ($\partial \bar{u}/\partial x < 0$) and the zonal elongated vorticity anomalies ($|u'^2| \gg |v'^2|$), positive CK is apt to be generated over the north China. Anomalous $\vec{E}$ fields with its axis tilted northeast to southwest in the entrance of the subtropical westerly jet ($\partial \bar{u}/\partial y > 0$) are the major contribution to negative CK over the east of northern China. The spatial distribution of CK can be a factor in the formation and maintenanance of the associated anomalous pattern (Kosaka and Nakamura 2006). As a result, during the high-correlation periods, the anomalies gain kinetic energy from the mean flow over the tropical and subtropical western Pacific, but release it to mean flow over the mid-latitudes in the lower troposphere, which is consistent with the propagation path of wave activity flux from the tropical to mid-latitudes (Fig. 5a). In the upper troposphere, the anomalies gain kinetic energy over northern China and release it over Japan. However, the CK pattern is weak in both the lower and upper levels during the low-correlation periods (Fig. 10c, d). The apparent difference of local barotropic energy conversion influences the intensity and maintenance of the associated anomalous pattern. In other words, during the high-correlation periods, the energy source of the related anomalies is partly provided by the stronger barotropic energy conversion.

As shown in Fig. 11, the baroclinic energy conversion into the associated anomalies mainly occurs in the exit region of Asian jet. With the meridional temperature gradient decreasing downstream along the exit of the subtropical jet, there is a distinct positive CP over the mid-latitude North China and a somewhat weaker negative CP over the North Japan during the high-correlation periods (Fig. 11a), leading to a net gain of available potential energy for the major cyclonic anomalies
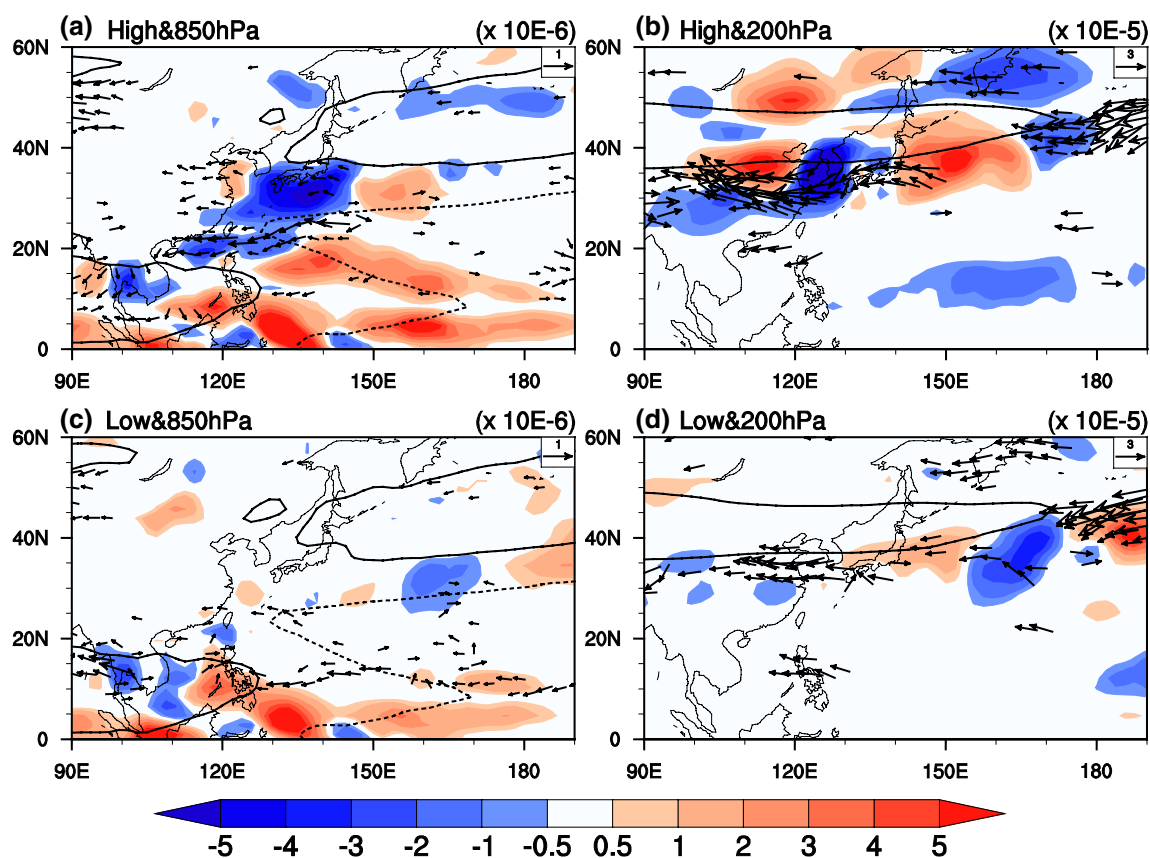
Fig. 10 The spatial distribution of local barotropic energy conversion (shaded; m^2s^{-3}) based on the JJA anomalous wind associated with DJF Niño-3.4 index and the corresponding extended EP flux [vector; (**a**)$\times 10^{-6}$ m^2s^{-2}, (**b**)$\times 10^{-5}m^2s^{-2}$] at **a** 850-hPa and **b** 200-hPa during the **a, b** high-correlation and **c, d** low-correlation periods. The contour indicates the regions of **a, c** $\bar{u} = \pm 4$ ms^{-1} and **b, d** $\bar{u} = \pm 25$ ms^{-1}, where dashed lines represent the negative value

Fig. 11 Vertically integrated baroclinic energy conversion (shaded; $\times 10^{-1}$ W m^{-2}) from the surface to 100-hPa level, superimposed on the climatological mean temperature at 400-hPa level (contours with interval 2K) during the **a** high-correlation and **b** low-correlation periods

(Figs. 3a, 4a). This characteristic is almost similar to the *CP* distribution in PJ pattern (Kosaka and Nakamura 2006). In contrast, the feature of *CP* is not obvious during the low-correlation periods (Fig. 11b), indicating weak local baroclinic energy conversion over the mid-latitudes. Therefore, the net gain of baroclinic energy over the

mid-latitudes is also a contributor to the maintenance of anomalous pattern during the high-correlation periods. The reason for the different distributions of *CK* and *CP* in the two periods can mainly be divided into two parts. First is caused by the anomalous fields, and the other is the contribution of the mean state fields. The results we found are investigated and discussed in the next subsection.

4.4 Mean state of winds

The change in location of anomalous convection over the western North Pacific may be related to the difference of mean state of summer winds between the two periods (Wu

and Wang 2002). In the 200-hPa level, the main characteristic of climatological wind shows a significant south Asia high (Fig. 12a). Difference between the two periods is mainly emerged as an anticyclone anomaly located in the western North Pacific (Fig. 12b), with the subtropical jet located to its north flank. This indicates an enhanced and northward displaced subtropical jet during the high-correlation periods. From the energy conversion point of view, the 200-hPa zonal elongated anticyclone discrepancy is prone to gaining energy. From the 500 and 850-hPa climatological wind, subtropical high is the dominant system. Similarly, an anticyclone anomaly is still the principle difference between the two periods. That is to say, the climatological
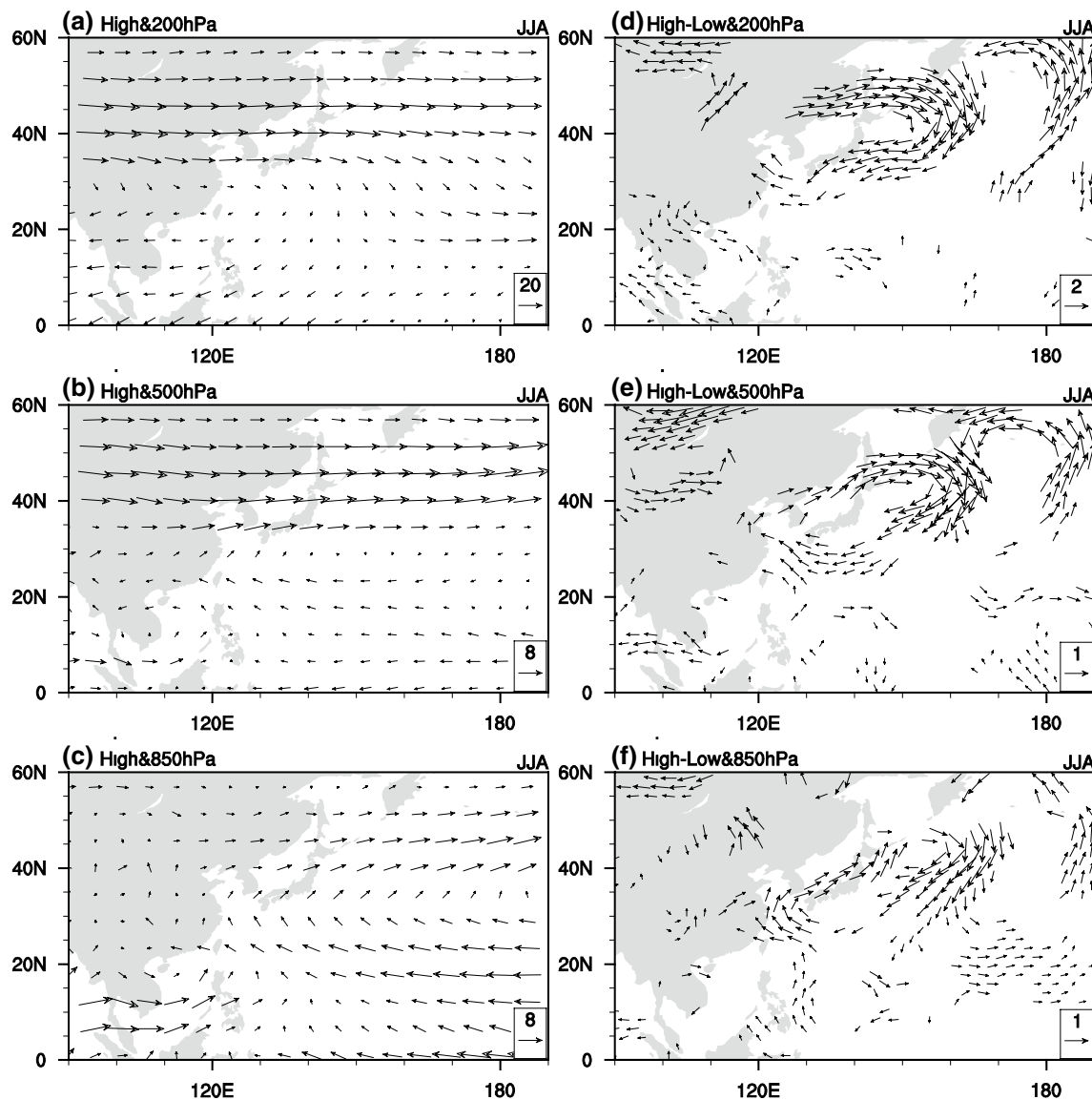
Fig. 12 The mean states of wind in **a** 200-hPa, **b** 500-hPa, and **c** 850-hPa levels during high-correlation periods, and their differences of **d** 200-hPa, **e** 500-hPa, and **f** 850-hPa mean JJA wind between high- and

low-correlation periods. The vector is shown when the meridional or zonal component is significant at the 5% level using Student's *t* test

subtropical high is also enhanced and displaced eastward to inland China. Although the apparent discrepancy exists in the mean state of winds between the two periods, we use the same anomalous fields related with the normalized previous winter Niño-3.4 index deriving from the high-correlation periods but different climate fields, which is respectively from the high- and low-correlation periods, to compute the impact of different climate states on the barotropic and baroclinic energy conversions (not shown). The results show relatively little disparity on their spatial distributions. Hence, although the climatological states have certainly difference, the amplitude of anomalous fields is the main reason for the discrepancies of circulation and precipitation over the East Asian-western North Pacific between the two periods. The interactions of climatological wind fields, ENSO and EASM, and how these affect the ENSO-EASM relationship, however, still need to be further investigated.

5 Conclusion and discussion

This study investigated the possible reason for the multi-decadal variations of the interannual relationship between ENSO and EASM in a 1000-year simulation of a coupled model. The results are further verified by AGCM experiences. The main findings are as the following.

The interannual relationship between ENSO and EASM is unstable and has significant multidecadal variations throughout the analysis period (1000-year). We selected two types of periods, one the high-correlation period and the other the low-correlation period, to document the differences in precipitation, atmospheric circulation, and SST anomalies. During the high-correlation periods, a tripolar precipitation anomaly pattern is significant from the tropical to the western North Pacific in the El Niño decaying summer. Besides an obvious warming over the India Ocean and apparent Matsuno-Gill pattern in troposphere geopotential height, the WPAC is intensified by the western tropical Pacific cooling and extends westwards to inland China. During the low-correlation periods, however, the tripolar anomalous precipitation pattern is weak and the Meiyu rain band located in the mid-latitude is absent. From the difference of anomalies of SST and other variables, the Indian Ocean warming is relatively weak and the western tropical Pacific cooling is not significant during the low-correlation periods, leading to weak WPAC. The ENSO-related anomalous SST difference between the two periods could be related to the pace of decay of ENSO events.

Using horizontal wave activity flux analysis, we can clearly see a perturbation in the western tropical Pacific in the lower troposphere during the high-correlation periods, and a significant tripolar vorticity anomaly pattern, the Rossby wave propagation northward to the subtropical jet area. In the upper troposphere, obvious Rossby wave propagates to the southeast, and a similar tripolar vorticity anomaly pattern exists though relatively weaker compared to lower troposphere. During the low-correlation periods, perturbation in the western tropical Pacific is weak and no significant wave-activity flux propagates to the north in the lower troposphere. Likewise, no wave-activity flux propagates in the upper troposphere.

In addition, comparison and analysis are made from the energy conversion point of view. During the high-correlation periods, significant positive barotropic energy conversion is present over the western tropical Pacific, indicating the conversion of kinetic energy from the mean flow to the anomalies associated with the DJF Niño-3.4 index. Hence, climate anomalous system in the lower troposphere over the tropics gains energy from the mean flow. In the upper troposphere over the mid-latitude around subtropical jet area, the anomalous system gains positive barotropic energy from the jet core, especially over northeast China. Moreover, there is a significant positive vertically integrated baroclinic energy conversion over the mid-latitude area. Therefore, the positive energy, including the barotropic and baroclinic energy, is attained to maintain the whole anomalous climate system. During the low-correlation periods, there is weak energy conversion from the mean flow to develop the associated anomalous system in the mid-latitude. The amplitude of anomalous fields is the main reason for the discrepancies of circulation and precipitation over the East Asian-western North Pacific between the two periods. Our results provide a good reference to ENSO impacts on East Asian summer climate on decadal timescales and it is also essential for climate prediction.

The applicability of the results obtained in the present study may depend upon the characteristics of the index used to describe the EASM variability. Zhao et al. (2015) showed that different EASM indices have different relation to tropical Indo-Pacific SST anomalies. Those indices that can capture the feature in the tropics may have a closer association with the tropical SST anomalies and thus the changes in the EASM-ENSO relationship and the plausible reasons as described in the present study may be captured to some extent. The EASM index of Huang and Yan (1999), which is defined based on 500 hPa geopotential height anomalies, appears to belong to this category. A parallel analysis shows that the EASM index of Huang and Yan (1999) captures the tripole anomalous rainfall pattern over the western Pacific and location of the WPAC. The associated SST anomalies in the high correlation periods are quite similar to those in the left column of Fig. 6. The difference of SST anomalies between the high and low correlation periods displays a distribution in the western North Pacific similar to that in the right column of Fig. 6 though with a smaller magnitude. In contrast, those indices that mainly describe the EASM

variability in the extratropics may have a weaker relationship to the tropical Indo-Pacific SST anomalies (Zhao et al. 2015) and consequently the changes in the EASM-ENSO relationship may be different from those obtained in the present study.

It is worth to mention that owing to the data we used here is the control simulation, so there is little change in mean state of SST during the two periods, which leads to little SST variations on the decadal time scales. Unlike other researches, the Pacific decadal oscillation (PDO) has little impacts on the discrepancy between the high- and low-correlation periods in our present study. Though significant difference exists between the two types of selected periods in our model, which seems to support the view that the decadal variation of ENSO-EASM relationship responds to natural variability, other issues that need to de further addressed are how does ENSO-EASM relationship change in response to anthropogenic or external forcing and what is the proportion of change accounted for by each forcing.

References

Bellenger H, Guilyardi E, Leloup J, Lengaigne M, Vialard J (2013) ENSO representation in climate models: from CMIP3 to CMIP5. Clim Dyn 42:1999–2018. doi:10.1007/s00382-013-1783-z

Chen LX, Dong M, Shao YN (1992) The Characteristics of interannual variations on the East-Asian monsoon. J Meteorol Soc Jpn 70:397–421

Compo GP et al (2011) The twentieth century reanalysis project. Q J Roy Meteor Soc 137:1–28. doi:10.1002/qj.776

Du Y, Xie SP, Huang G, Hu KM (2009) Role of air–sea interaction in the long persistence of El Nino-induced North Indian ocean warming. J Clim 22:2023–2038. doi:10.1175/2008JCLI2590.1

Gill AE (1980) Some Simple solutions for heat-induced tropical circulation. Q J Roy Meteor Soc 106:447–462. doi:10.1256/Smsqj.44904

Gong H, Wang L, Chen W, Nath D, Huang G, Tao W (2015) Diverse influences of ENSO on the East Asian–Western Pacific winter climate tied to different ENSO properties in CMIP5 models. J Clim 28:2187–2202. doi:10.1175/jcli-d-14-00405.1

Gualdi S, Navarra A, Guilyardi E, Delecluse P (2003) Assessment of the tropical Indo-Pacific climate in the SINTEX CGCM. Ann Geophys Italy 46:1–26

He Z, Wu R (2013) Seasonality of interannual atmosphere-ocean interaction in the South China Sea. J Oceanography 69(6):699–712. doi:10.1007/s10872-013-0201-9

Hoskins BJ, James IN, White GH (1983) The shape, propagation and mean-flow interaction of large-scale weather systems. J Atmos Sci 40:1595–1612. doi:10.1175/1520-0469(1983)040<1595:Tspamf>2.0.Co;2

Hu K, Huang G, Zheng X-T, Xie S-P, Qu X, Du Y, Liu L (2014) Interdecadal variations in ENSO influences on Northwest

Pacific–East Asian early summertime climate simulated in CMIP5 models. J Clim 27:5982–5998. doi:10.1175/jcli-d-13-00268.1

Huang G, Yan ZW (1999) The East Asian summer monsoon circulation anomaly index and its interannual variations. Chin Sci Bull 44:1325–1329. doi:10.1007/Bf02885855

Huang G, Hu K, Xie S-P (2010) Strengthening of tropical Indian Ocean teleconnection to the Northwest pacific since the Mid-1970s: an atmospheric GCM study. J Clim 23:5294–5304. doi:10.1175/2010jcli3577.1

Huang P, Wang P, Hu K, Huang G, Zhang Z, Liu Y, Yan B (2014) An Introduction to the integrated climate model of the center for monsoon system research and its simulated influence of El Niño on East Asian-western North Pacific CLIMATE. Adv Atmos Sci 31:1136–1146. doi:10.1007/s00376-014-3233-1

Jiang W, Huang G, Hu K, Wu R, Gong H, Chen X, Tao W (2017) Diverse relationship between ENSO and the Northwest Pacific summer climate among CMIP5 models: dependence on the ENSO decay pace. J Clim 30:109–127. doi:10.1175/jcli-d-16-0365.1

Kim ST, Yu J-Y (2012) The two types of ENSO in CMIP5 models. Geophys Res Lett. doi:10.1029/2012gl052006

Kosaka Y, Nakamura H (2006) Structure and dynamics of the summertime Pacific–Japan teleconnection pattern. Q J Roy Meteor Soc 132:2009–2030. doi:10.1256/qj.05.204

Liu B, Huang G, Wang PF, Yan BL, Zhao GJ (2017) The dependence on atmospheric resolution of ENSO and related East Asian-Western North Pacific Summer climate variability in a coupled model. Theor Appl Climatol. doi:10.1007/s00704-017-2254-y

Luo JJ, Masson S, Roeckner E, Madec G, Yamagata T (2005) Reducing climatology bias in an ocean-atmosphere CGCM with improved coupling physics. J Clim 18:2344–2360. doi:10.1175/Jcli3404.1

Madec G (2008) NEMO ocean engine. Note du Pole de modelisation 27. Institut Pierre-Simon Laplace, pp 193

Matsuno T (1996) Quasi-geostrophic motions in the equatorial area. J Meteor Soc Jpn 44:25–43

Nitta T (1987) Convective activities in the tropical western Pacific and their impact on the Northern Hemisphere summer circulation. J Meteor Soc Japan 65:373–390

Park W, Keenlyside N, Latif M, Ströh A, Redler R, Roeckner E, Madec G (2009) Tropical pacific climate and its response to global warming in the Kiel climate model. J Clim 22:71–92. doi:10.1175/2008jcli2261.1

Roeckner E, Coauthos (2003) The atmospheric general circulation model ECHAM5. PART I: model description. Report 349, Max Planck Institute for Meteorology, p 140

Roeckner E et al (2006) Sensitivity of simulated climate to horizontal and vertical resolution in the ECHAM5 atmosphere model. J Clim 19:3771–3791. doi:10.1175/Jcli3824.1

Simmons AJ, Wallace JM, Branstator GW (1983) Barotropic wave-propagation and instability, and atmospheric teleconnection patterns. J Atmos Sci 40:1363–1392. doi:10.1175/1520-0469(1983)040<1363:Bwpaia>2.0.Co;2

Song FF, Zhou TJ (2014) Interannual variability of East Asian Summer monsoon Simulated by CMIP3 and CMIP5 AGCMs: skill dependence on indian ocean-Western Pacific anticyclone teleconnection. J Clim 27:1679–1697. doi:10.1175/Jcli-D-13-00248.1

Song FF, Zhou T (2015) The Crucial role of internal variability in modulating the decadal variation of the East Asian Summer Monsoon–ENSO Relationship during the twentieth century. J Clim 28:7093–7107. doi:10.1175/jcli-d-14-00783.1

Takaya K, Nakamura H (2001) A formulation of a phase-independent wave-activity flux for stationary and migratory quasigeostrophic eddies on a zonally varying basic flow. J Atmos Sci 58:608–627. doi:10.1175/1520-0469(2001)058<0608:Afoapi>2.0.Co;2

Tao W, Huang G, Hu K, Gong H, Wen G, Liu L (2015) A study of biases in simulation of the Indian Ocean basin mode and its capacitor effect in CMIP3/CMIP5 models. Clim Dyn 46:205–226. doi:10.1007/s00382-015-2579-0

Valcke S (2006) OASIS3 user guide. PRISM Tech Rep 3:64

Wang B, Wu RG, Fu XH (2000) Pacific-East Asian teleconnection: how does ENSO affect East Asian climate? J Clim 13:1517–1536. doi:10.1175/1520-0442(2000)013<1517:Peathd>2.0.Co;2

Wang B, Wu RG, Li T (2003) Atmosphere-warm ocean interaction and its impacts on Asian-Australian monsoon variation. J Clim 16:1195–1211. doi:10.1175/1520-0442(2003)16<1195:Aoiaii>2.0.Co;2

Wang B, Wu Z, Li J, Liu J, Chang C-P, Ding Y, Wu G (2008a) How to measure the strength of the East Asian summer monsoon. J Clim 21:4449–4463. doi:10.1175/2008jcli2183.1

Wang B, Yang J, Zhou T, Wang B (2008b) Interdecadal changes in the major modes of Asian–Australian Monsoon variability: strengthening relationship with ENSO since the Late 1970s. J Clim 21:1771–1789. doi:10.1175/2007jcli1981.1

Wu R, Kirtman BP (2003) On the impacts of the Indian summer monsoon on ENSO in a coupled GCM. Q J Roy Meteor Soc 129:3439–3468. doi:10.1256/qj.02.214

Wu R, Wang B (2002) A contrast of the east Asian summer monsoon-ENSO relationship between 1962-77 and 1978-93. J Clim 15:3266–3279. doi:10.1175/1520-0442(2002)015<3266:Acotea>2.0.Co;2

Wu R, Kirtman BP, Krishnamurthy V (2008) An asymmetric mode of tropical Indian Ocean rainfall variability in boreal spring. J Geophys Res Atmos. doi:10.1029/2007jd009316

Wu B, Zhou TJ, Li T (2009) Seasonally evolving dominant interannual variability modes of East Asian climate. J Clim 22:2992–3005. doi:10.1175/2008JCLI2710.1

Wu R, Huang G, Du Z, Hu K (2014) Cross-season relation of the South China Sea precipitation variability between winter and summer. Clim Dyn 43(1–2):193–207. doi:10.1007/s00382-013-1820-y

Xie X, Philander SGH (1994) A coupled ocean-atmosphere model of relevance to the itcz in the eastern pacifc. Tellus A Dyn Meteorol Oceanogr 46:340–350. doi:10.1034/j.1600-0870.1994.t01-1-00001.x

Xie SP, Hu KM, Hafner J, Tokinaga H, Du Y, Huang G, Sampe T (2009) Indian ocean capacitor effect on Indo-Western Pacific climate during the summer following El Nino. J Clim 22:730–747. doi:10.1175/2008JCLI2544.1

Xie SP, Du Y, Huang G, Zheng X-T, Tokinaga H, Hu K, Liu Q (2010) Decadal shift in El Niño Influences on Indo–Western Pacific and East Asian climate in the 1970s. J Clim 23:3352–3368. doi:10.1175/2010jcli3429.1

Xie SP, Kosaka Y, Du Y, Hu KM, Chowdary J, Huang G (2016) Indo-western Pacific ocean capacitor and coherent climate anomalies in post-ENSO summer: a review. Adv Atmos Sci 33:411–432. doi:10.1007/s00376-015-5192-6

Yang JL, Liu QY, Xie SP, Liu ZY, Wu LX (2007) Impact of the Indian Ocean SST basin mode on the Asian summer monsoon. Geophys Res Lett 34:L02708. doi:10.1029/2006gl028571

Zhang RH, Sumi A, Kimoto M (1996) Impact of El Nino on the East Asian monsoon: A diagnostic study of the '86/87 and '91/92 events. J Meteorol Soc Jpn 74:49–62

Zhang RH, Sumi A, Kimoto M (1999) A diagnostic study of the impact of El Nino on the precipitation in China. Adv Atmos Sci 16:229–241. doi:10.1007/Bf02973084

Zhang RH, Min Q, Su J (2017) Impact of El Niño on atmospheric circulations over East Asia and rainfall in China: role of the anomalous western North Pacific anticyclone. Sci China Earth Sci 60:1124–1132. doi:10.1007/s11430-016-9026-x

Zhao G, Huang G, Wu R, Tao W, Gong H, Qu X, Hu K (2015) A new upper-level circulation index for the East Asian summer monsoon variability. J Clim 28:9977–9996. doi:10.1175/jcli-d-15-0272.1